Upper crustal velocity and seismogenic environment of the *M*7.0 Jiuzhaigou earthquake region in Sichuan, China

DaHu Li[1]*, ZhiFeng Ding[2], Yan Zhan[3], PingPing Wu[3], LiJun Chang[2], and XiangYu Sun[3]

[1]Chengdu Institute of the Tibetan Plateau Earthquake Research, China Earthquake Administration, Chengdu 610041, China;

[2]Institute of Geophysics, China Earthquake Administration, Beijing 100081, China;

[3]Institute of Geology, China Earthquake Administration, Beijing 100029, China

Key Points:
- The P-wave velocity structure of the upper crust around the Jiuzhaigou earthquake region shows obvious lateral inhomogeneity, low-velocity anomalies are observed at the intersection of shallow part of Minjiang and Tazang faults.
- The relocated earthquake sequence distributed along the NW-SE direction and ends near the intersection of the Minjiang and Tazang faults, the inhomogeneous variation of the velocity structure of the Jiuzhaigou earthquake region and its surrounding medium is the deep structural factor controlling the spatial distribution of the mainshock and its sequence.
- The crustal low-velocity layer of northeastern Songpan–Garzê Block stretches into Minshan Mountain, and migrates to the northeast, the tendency to emerge as a shallow layer is impeded by the high velocity zone of Nanping Nappe tectonics and Bikou Block.

Citation: Li, D. H., Ding, Z. F., Zhan, Y., Wu, P. P., Chang, L. J. and Sun, X. Y. (2021). Upper crustal velocity and seismogenic environment of the *M*7.0 Jiuzhaigou earthquake region in Sichuan, China. *Earth Planet. Phys.*, *5*(4), 348–361. http://doi.org/10.26464/epp2021038

Abstract: On August 8, 2017, a magnitude 7.0 earthquake occurred in Jiuzhaigou County, Sichuan Province, China. The deep seismogenic environment and potential seismic risk in the eastern margin of Tibetan Plateau have once again attracted the close attention of seismologists and scholars at home and abroad. The post-earthquake scientific investigation could not identify noticeable surface rupture zones in the affected area; the complex tectonic background and the reason(s) for the frequent seismicity in the Jiuzhaigou earthquake region are unclear. In order to reveal the characteristics of the deep medium and the seismogenic environment of the *M*7.0 Jiuzhaigou earthquake region, and to interpret the tectonic background and genesis of the seismicity comprehensively, in this paper, we have reviewed all available observation data recorded by the regional digital seismic networks and large-scale, dense mobile seismic array (China Array) for the northern section of the North–South Seismic Belt around Jiuzhaigou earthquake region. Using double-difference seismic tomography method to invert the three-dimensional P-wave velocity structure characteristics of the upper crust around the Jiuzhaigou earthquake region, we have analyzed and discussed such scientific questions as the relationship between the velocity structure characteristics and seismicity in the Jiuzhaigou earthquake region, its deep tectonic environment, and the ongoing seismic risk in this region. We report that: the P-wave velocity structure of the upper crust around the Jiuzhaigoug earthquake region exhibits obvious lateral inhomogeneity; the distribution characteristics of the shallow P-wave velocity structure are closely related to surface geological structure and formation lithology; the *M*7.0 Jiuzhaigou earthquake sequence is closely related to the velocity structure of the upper crust; the mainshock of the *M*7.0 earthquake occurred in the upper crust; the inhomogeneous variation of the velocity structure of the Jiuzhaigou earthquake area and its surrounding medium appears to be the deep structural factor controlling the spatial distribution of the mainshock and its sequence. The 3D P-wave velocity structure also suggests that the crustal low-velocity layer of northeastern SGB (Songpan–Garzê Block) stretches into MSM (Minshan Mountain), and migrates to the northeast, but the tendency to emerge as a shallow layer is impeded by the high-velocity zone of Nanping Nappe tectonics and the Bikou Block. Our results reveal an uneven distribution of high- and low-velocity structures around the Tazang segment of the East Kunlun fault zone. Given that the rupture caused by the Jiuzhaigou earthquake has enhanced the stress fields at both ends of the seismogenic fault, it is very important to stay vigilant to possible seismic hazards in the large seismic gap at the Maqu–Maqên segment of the East Kunlun fault zone.

Keywords: the *M*7.0 Jiuzhaigou earthquake; 3D P-wave velocity structure; deep tectonic; seismogenic environment

1. Introduction
On August 8, 2017, the China Earthquake Networks Center (CENC)

recorded an *M*7.0 earthquake at Jiuzhaigou County (33.22°N, 103.83°E, hereinafter Jiuzhaigou earthquake) of Aba, Sichuan Province, at 21:19:46.4 Beijing time. The earthquake involved a sequence of active events. Between August 8 and 14, 2017, the Sichuan Regional Seismic Network recorded 3812 earthquake events of magnitude $M_L \geq 0.0$ in the Jiuzhaigou earthquake sequence. Among them, 1369 earthquake events were of M_L 0.0–0.9,

1876 events of M_L 1.0–1.9, 416 events of M_L 2.0–2.9, 59 events of M_L 3.0–3.9, 14 events of M_L 4.0–4.9, and 1 event of M_L 7.0–7.9. The strongest aftershock was the M4.8 earthquake on August 9, 2017. The M7.0 Jiuzhaigou earthquake caused 25 deaths and 525 injuries, with six people missing. About 176,492 people were affected by the disaster and 73,671 houses were damaged to varying degrees. After the earthquake, the seismic investigation team of Sichuan Earthquake Administration conducted a field investigation in the affected areas and determined the intensity distribution of the earthquake based on a comprehensive evaluation of the tectonic setting of the affected regions, the distribution of aftershocks, and strong motion observations (Jiuzhaigou earthquake Intensity Distribution Map, Seismological Bureau of Sichuan Province, 2017). The isoseismals are elliptical. The long axis is NNW-trending, which is roughly the same as the distribution of the aftershocks. The short axis is near-NE and approximately 160-km long. An area 19 km long sustained extreme earthquakes of intensity Ⅸ; a 45 km-long region was affected by intensity Ⅷ events (Yi GX et al., 2017).

Following the M8.0 Wenchuan earthquake of 2008 and M7.0 Lush-

an earthquake of 2013, the M7.0 Jiuzhaigou earthquake of 2017 was the third destructive earthquake event in the eastern margin of the Tibetan Plateau to have occurred within a decade. With regard to regional tectonics, the epicenter of the M7.0 Jiuzhaigou earthquake was in the eastern part of the Bayan Har Block, at the intersection of the eastern segment of the East Kunlun fault zone and the Minjiang tectonic belt (Figure 1). At its epicenter and surrounding areas are the NWW-trending Tazang fault at the eastern segment of the East Kunlun fault zone, the NNW-trending Huya fault, and the near NS-trending Minjiang fault. These faults form the north and east boundaries of the Bayan Har Block; in terms of neotectonics, they also constitute the horsetail-shaped structure spreading out toward the east or southeast at the eastern tip of the NWW-trending East Kunlun fault zone (Xu XW et al., 2017a; Yi GX et al., 2017).

The eastern segment of the East Kunlun fault close to the epicenter of the Jiuzhaigou earthquake starts in the west at the northeast of the Zoige Basin and extends SEE-ward to the north of Minshan Mountain. It has a reversed S-shape structure, showing new activities that apparently belong to the Late Quaternary. Its tip is
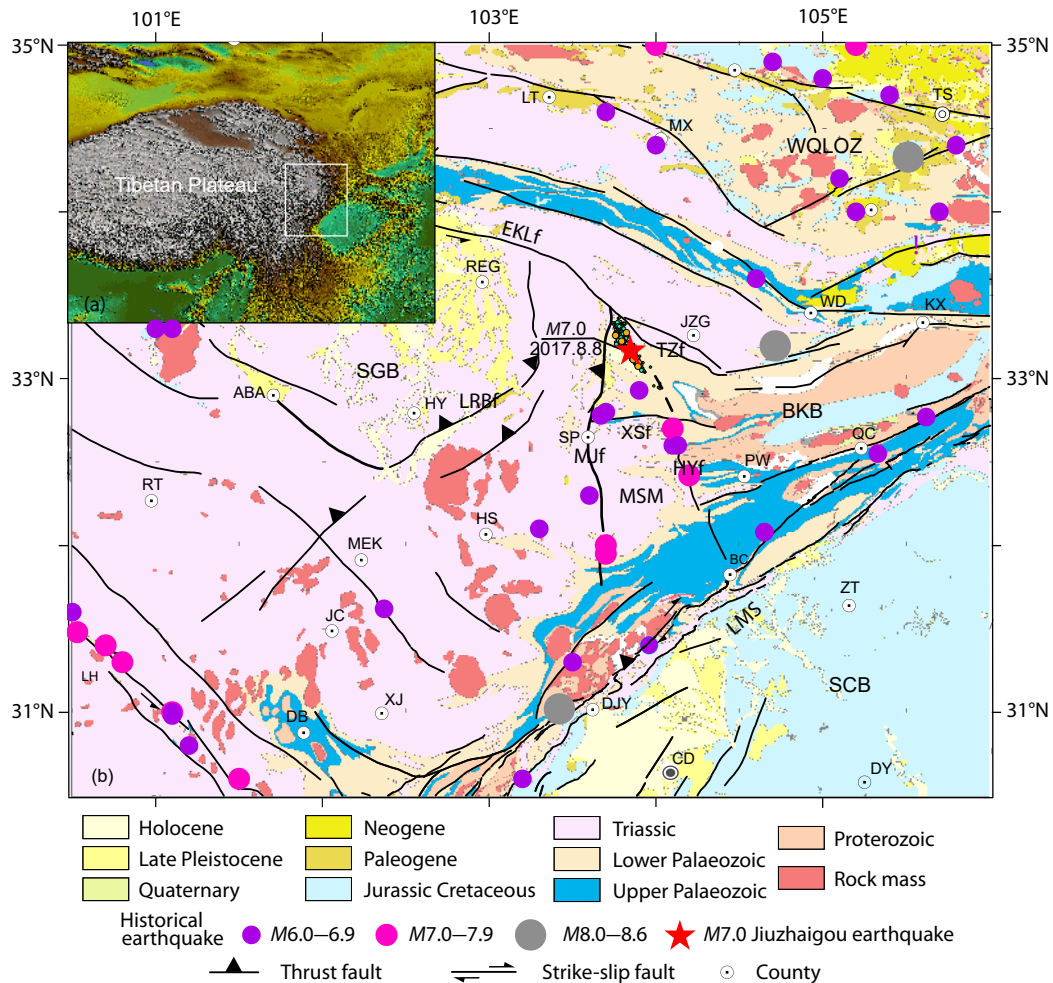

Figure 1.   (a) Sketch map of the research area. (b) Seismotectonic setting of the M7.0 Jiuzhaigou earthquake region and its adjacent area. The abbreviations are: EKLf, Easternmost Kunlun fault; MJf, Minjiang fault; XSf, Xueshan fault; HYf, Huya fault; LRBf, Longriba fault; WQLOZ, West Qinling Orogenic zone; SGB, Songpan–Garzê Block; BKB, Bikou Block; LMS, Longmen Shan; SCB, Sichuan Basin; MSM, Minshan Mountain. The red star denotes the location of the M7.0 Jiuzhaigou mainshock.

split into numerous secondary faults, giving rise to horsetail-shaped or broom-like structures (Cunningham and Mann, 2007; Li CX et al., 2011). The Minshan tectonic belt, located to the south of the East Kunlun fault zone, consists primarily of the near NS-trending Minjiang fault, NNW-trending Huya fault zone, and near EW-trending Xueshan fault. The Minjiang and Huya faults form the west and east boundaries of the Minshan tectonic belt; both are active faults of the Holocene. They have dictated the geomorphological evolution of the MSM since the Quaternary Period (Zhao XL et al., 1994; Zhang HP et al., 2006). There have been several intense and large-scale earthquakes in the Minshan fault, such as the *M*7 Diexi earthquake in 1713, the *M*6½ North Zhangla earthquake in 1748, the *M*6 Songpan earthquake in 1938, the *M*6¾ Zhangla earthquake in 1960, and the *M*7½ Diexi earthquake in 1933. Two *M*7.2 earthquake events occurred along the Huya fault in 1976.

Recently, many important results have been obtained by geoscientists in their studies of the Jiuzhaigou earthquake region and its surrounding areas. Using the focal mechanism and the distribution of relocated aftershocks, Yi GX et al. (2017) suggested that the mainshock of the *M*7.0 Jiuzhaigou earthquake was generated on the NW-SE-trending Shuzheng fault, between the Minjiang and Tazang faults. Ji LY et al. (2017) obtained the coseismic deformation fields of the Jiuzhaigou earthquake using InSAR, which exhibited an asymmetric distribution that they attributed to differences in the medium properties and deep pitches of the hanging wall and footwall of the seismogenic fault. Using seismic records from stations in the affected area, Yang Y and Chang LJ (2018) studied the spatial and temporal variation of shear wave splitting of the *M*7.0 Jiuzhaigou earthquake sequence and observed partitioning in the fast polarization directions of the upper crust. Zhang X et al. (2017), Xu LS et al. (2018), Liang JH et al. (2018), Fang LH et al. (2018), Liang SS et al. (2018), and Long F et al. (2019) determined precise positioning of the mainshock and aftershocks of the earthquake. The Jiuzhaigou earthquake happened in a region characterized by high mountains and deep valleys, on which a few geological and geophysical studies have been conducted. Furthermore, the post-earthquake scientific investigation could not identify noticeable surface rupture zones in the affected area. These factors have limited study of the event's seismogenic mechanism and the main cause of the rupture process. Thus, the complex tectonic background of the Jiuzhaigou earthquake region and the reason for its frequent seismicity remain unclear.

The development and occurrence of strong earthquakes involve the dynamics or tectonic movement of Earth's interior. The occurrence is closely related to the deep structure, physical properties, and dynamic environment of the crust and upper mantle (Ding ZF, 2011; Xu T et al., 2014). The velocity structure of the crust is an important parameter that reflects the properties of the crustal medium. The characteristics of the 3D velocity structure, closely related to tectonic movement, provide important information about the location of an earthquake and the source medium. Combined with the spatial distribution of seismic activities, the velocity structure serves as an important basis for understanding the environment and mechanism of earthquake occurrence (Zhao CP, 2006). In this study, observation data recorded by the regional digital seismic networks of Sichuan, Gansu, Qinghai, and Shaanxi provinces from January, 2013, to July 2019 were collected. The waveform data were recorded by the large-scale, dense mobile seismic array (China Array) for the northern section of the North–South Seismic Belt from Sep, 2013, to Aug 2015 (Figure 2). P-wave data were extracted from the waveform data; double-difference tomography (TOMODD) was used to retrieve 3D P-wave velocity structures for the upper crust of the areas affected by the *M*7.0 Jiuzhaigou earthquake region and its adjacent areas. The relationship between velocity structure and seismicity, deep seismogenic environment, and seismic hazard risk are discussed. The results obtained form the basis for understanding the dynamic mechanism of earthquake development in the Minshan area (as part of the eastern margin of Tibetan Plateau), forecasting seismic activity trends and seismic hazard risks in the region. These res-
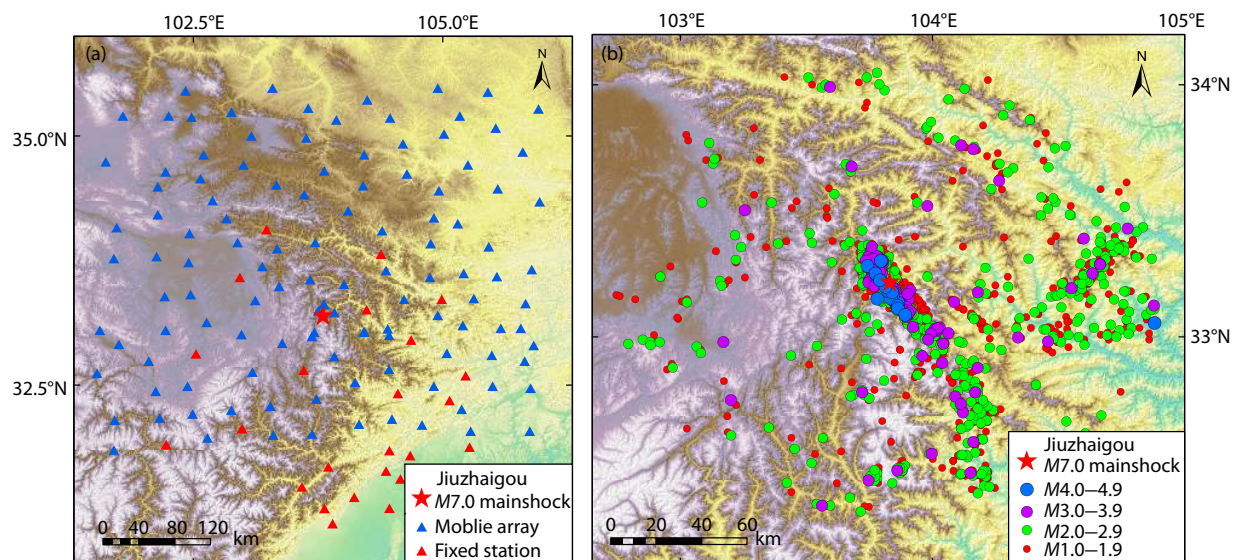

Figure 2.   (a) Distribution map of seismic stations and (b) earthquake epicenters used in this study.

Li DH et al.: Upper crustal velocity of the *M*7.0 Jiuzhaigou earthquake region

ults should help to minimize the damage caused by future such disasters.

2. Data and Imaging Method

2.1 Data Collection

The Sichuan Earthquake Administration and Gansu Earthquake Administration started the set-up of mobile seismic stations in the Jiuzhaigou earthquake region on the same day the Jiuzhaigou earthquake happened. As of August 12, 2017, six mobile seismic stations had been installed in the vicinity of the earthquake area, four by Sichuan Earthquake Administration (Stations L5110, L5111, L5112, and L5113; sampling rate: 100 Hz) and two by Gansu Earthquake Administration (Stations L6201 and L6202; sampling rate: 100 Hz). Stations L5510, L5511, and L5512 were equipped with CMG-40TDE (2s–50Hz) short-period seismometers, whereas Stations L5113, G6201, and G6202 were equipped with GL-PS2 (2s–50Hz) short-period seismometers. Observation data recorded by the mobile stations were transmitted to the Sichuan Earthquake Administration in real-time (Figure 2a). In this study, we collected seismic data from 25 fixed seismic stations in the Jiuzhaigou earthquake region and its surroundings. In addition, seismic event records from 119 sets of seismic monitoring equipment were adopted, including 113 sets from the dense mobile seismic array deployed by the China Array for the northern section of the North–South Seismic Belt and 6 sets from the earthquake mobile observation station. As shown in Figure 2b, the seismic stations in and around the Jiuzhaigou earthquake region form a dense distribution, covering a large range of azimuthal angles in the study area. This ensures the completeness of the earthquake sequence catalog, as well as density of ray intersections and reliability of the inversion from imaging data.

Before performing the inversion, the P-wave arrival times were scrutinized during data preprocessing. Using the seismic phase travel time vs epicentral distance curve, only seismic events with $M_L \geq 1.0$ were selected from the recorded data. Seismic phases whose travel-time curves were characterized by large dispersion were eliminated; for each seismic event, at least five stations had collected P-wave arrival time data (Figure 3). Within one month after the Jiuzhaigou earthquake, more than 3000 events occurred in the area. The seismic sequence forms a NWW-trending belt. The large number of seismic events occurring in and around the Jiuzhaigou earthquake region and their dense ray intersections provide adequate data for the retrieval of the velocity structure in the earthquake area (Figure 4).

2.2 Imaging Method

We used the TOMODD method to retrieve the 3D P-wave velocity structure of the Jiuzhaigou earthquake region (Zhang HJ and Thurber, 2003, 2006). Based on the double-difference earthquake location algorithm, this method uses both relative and absolute travel-time data in its joint inversion of 3D velocity structures and source locations (Waldhauser and Ellsworth, 2000). Absolute travel times are the primary basis for determining the 3D velocity structure of the entire study area. For better constraint of the 3D velocity structure and source location, relative travel times are assigned more weight after the iteration steps. Compared to tradi-
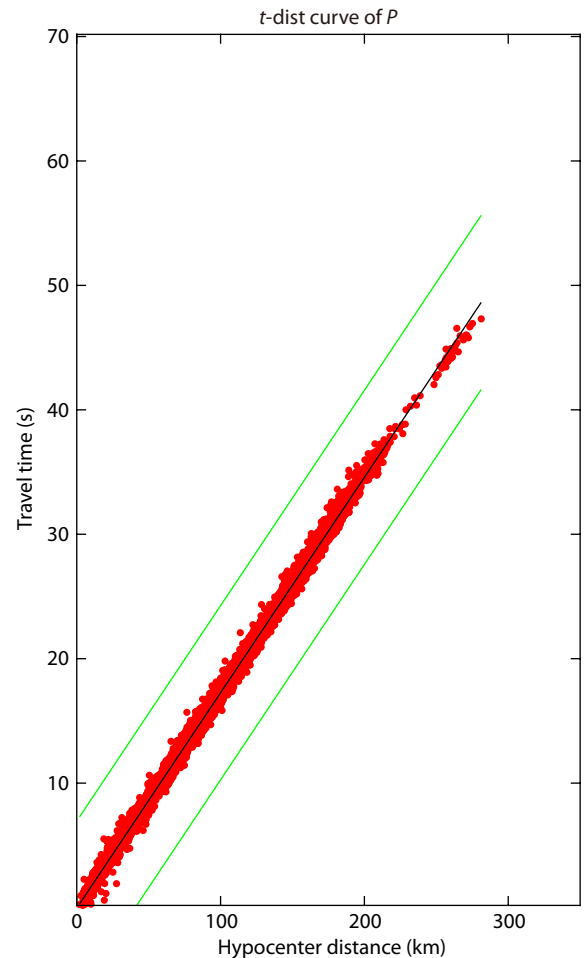

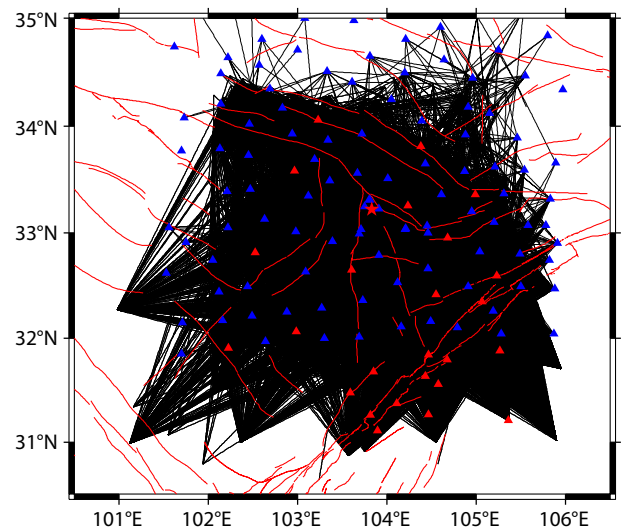**Figure 3**. The fitting curve of travel time and epicentral distance.

Figure 4. Distribution of P-wave ray paths used in this study. The red star denotes the location of the M7.0 Jiuzhaigou mainshock.

tional travel-time-based tomography methods, TOMODD considers variations in the velocity structure of underground media and gets around the assumption in the double-difference location algorithm that the travel velocities of a pair of events to a common seismic station are the same. Incorporating relative

travel time in the inversion, the accuracy of the retrieved 3D velocity structure is also improved; thus, more fine structure of the underground media can be recovered. This method has become widely used recently in determining 3D velocity structure inversion in different regions (Thurber et al., 2004, 2007; Okada et al., 2006, 2007; Hofstetter et al., 2012; Allam et al., 2014; Wu HB et al., 2018; Watkins et al., 2018; Li DH et al., 2021). When matching earthquake event pairs, the maximum distance between event pairs were set to 10 km; every earthquake event was matched to more than 30 other events. Finally, from the 7126 seismic events a total of 22,438 absolute arrival-times and 1,268,643 relative arrival-times were selected for joint inversion. Based on the distribution of seismic events, location of seismic stations, and coverage of seismic rays in the Jiuzhaigou earthquake region, the study area was divided into grids. The center of the study area (Jiuzhaigou earthquake region and its vicinity) and the edges were divided into 0.1° × 0.1° and 0.2° × 0.2° grids, respectively, in the lateral direction. In the vertical direction, divisions were made at 1, 3, 6, 9, 12, 15, 18, and 21 km. The Crust1.0 crustal velocity model and PREM model were used to establish a one-dimensional (1D) initial P-wave velocity model for the study area.

2.3 Parameter Selection

During inversion, a damped LSQR algorithm (least-squares QR factorization) was adopted to solve least-squares problems with damping. The 2-norm of the total travel-time residual was employed as the objective function for iterating and solving the equations (Zhang HJ and Thurber, 2003). During imaging, the change in slowness was constrained by smoothing factors, whereas the change in earthquake location and slowness was constrained by damping factors. Because the stability of inversion results is largely dependent on the magnitude of the smoothing and damping factors, it is particularly important to examine the choice of damping and smoothing factors before inversion (Eberhart-Phillips, 1986, 1993; Ma X et al., 2016). To this end, a curve of the

model variance vs. data variance was plotted to ensure the stability of the inversion results. The parameter combination corresponding to significantly minimized data variance and minimal change in model variance was selected as the optimal parameters for inversion. The L-curve was employed to obtain the optimal parameters (Hansen, 1992; Hansen and O'Leary, 1993). The search range of the smoothing factor was 10–400 and that of the damping factor was 50–1000. The optimal smoothing and damping factors were obtained as 40 and 300, respectively (Figure 5). After 20 iterations, the mean square deviation in travel-time residual decreased from 0.27 to 0.04 s. Figure 6 shows the statistical distribution of residuals before and after inversion. As seen in Figure 6, the residuals are concentrated at −1.5 to 1.5 s before inversion. After the inversion, the distribution of the residuals changes; the values start to converge to the center and are now mainly concentrated at −0.5 to 0.5 s. This means that the velocity model obtained by this inversion method provides a good fit of the observation data.

2.4 The Checkerboard Test

The checkerboard test was used to evaluate the reliability and spatial resolution of the velocity structure retrieved (Spakman et al., 1993). Alternating positive and negative velocity perturbations were introduced into the initial model to generate the checkerboard and compute the theoretical travel time. Inversion was then performed using the initial model and theoretical travel-time data. The inversion results were then evaluated with regard to their ability to restore the checkerboard. Regions with better perturbation recovery indicate reliable inversion results. Forward modeling of theoretical travel time was performed using a checkerboard with grid divisions, as described in Section 2.2, and ± 3% velocity perturbations. The theoretical travel-time data generated were used with the actual initial model for inversion. Figure 7 shows the inversion results at different depths, which show good recovery of the checkerboard at the center of the study area, with
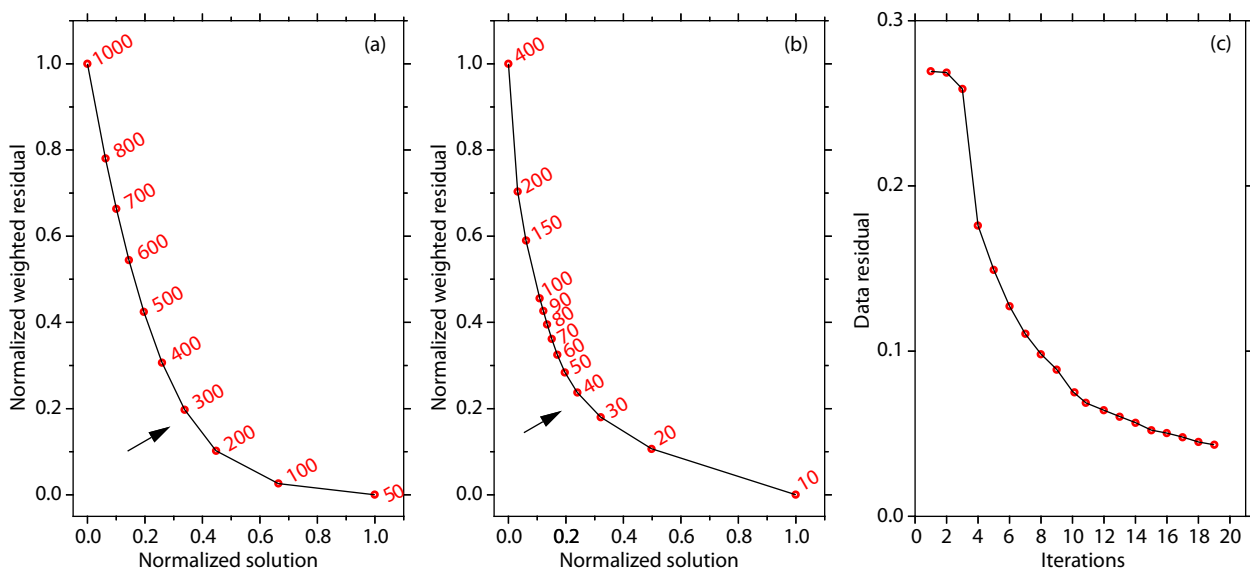

Figure 5. (a) The damping parameter selected by L-curve; (b) The optimum smoothing parameter selected by L-curve; and (c) The data residual versus iteration number.
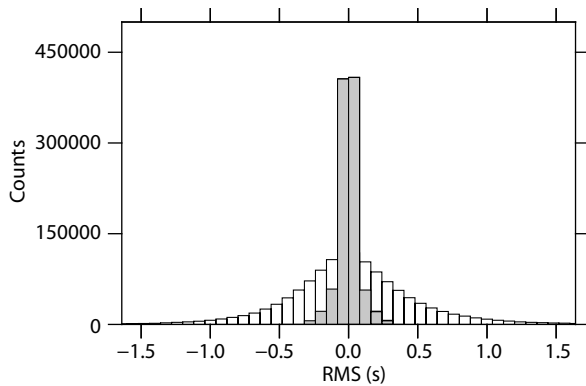
Figure 6. P waves residual distribution before and after inversion. The white box represents the residual before inversion, and the gray box represents the residual after inversion.

a resolution of 0.1° × 0.1° achieved in the tomography results. This high resolution is due primarily to the concentration of seismic events in the Jiuzhaigou earthquake region and the large number of seismic rays present in the upper crust.

3. Characteristics of P-wave Velocity Structure

The study area encompasses the northeastern part of Songpan–Garzê Block (SGB), the southern rim of West Qinling Orogenic Zone (WQLOZ), Minshan Mountain (MSM), and the Bikou Block (BKB). Figure 8 shows the 3D P-wave anomaly distribution at depths of 1–18 km. A noticeable lateral inhomogeneity is observed in the crustal P-wave velocity structure. This indicates the significant medium differences in the lateral direction for the upper crustal materials in the Jiuzhaigou earthquake region. The 1 km velocity structure plot shows that the distribution characteristics of the shallow P-wave velocity structure are closely related to the surface geological structure and formation lithology (Figure 8a). The Remoke–Sangri region in the northeastern SGB and Nanping Nappe at the southern end of WQLOZ are all located in high-velocity regions. The overlaying stratum on the surface of SGB is composed mainly of Triassic flysch (Sun JB et al., 2018). The exposed strata in Aba Sag consist primarily of Triassic Zagunao and Zhuwo Formations, with occasional exposure of Middle Triassic strata at the axis of the anticline. Esitic tuff and tuffite with a thickness of nearly 100 m are found in the eastern part of the Tazang–Longkang Profile of Nanping Nappe at the southern end of WQLOZ (Qin JF et al., 2008). Based on the above observations, the distribution of high-velocity anomalies in the shallow layer is assumed to be closely related to the distribution of stratum lithology in this region. Sandwiched between the Minjiang and Huya faults is MSM, with a complex deep velocity structure characterized by trap- or strip/belt-like distributions. The region north of the eastwest trending Xueshan fault features alternating high and low velocities. Huya fault, extending in the NNW direction, forms the east boundary of the Minshan Mountains. To the east of this fault are the middle and low altitude mountain areas with a planation surface of about 3200–3500 m in altitude. To its west is the Minshan Mountain with a planation surface of about 4200–4500 m in altitude. Due to the west-eastward thrust of the Huya fault, the planation surfaces on the east and west are vertically dis-

placed by about 1000 m. Thus, the east and west sides of the northern section of the Huya fault show low- and high-velocity structures, respectively. Noticeable trap-like low-velocity structures are observed at the intersection of Minjiang and Tazang faults and in the western part of BKB. This is consistent with the low resistivity of the shallow crust revealed by magnetotelluric inversion results obtained in this region (Min G et al., 2017; Sun XY et al., 2020).

The velocity structure distribution at a depth of 3 km reveals even more prominent velocity structures. A high-velocity anomaly persists within MSM and Nanping Nappe tectonics, and the low-velocity anomaly in the western part of BKB gradually enlarges. A division line between high- and low-velocity anomalies is found near the northern segment of Huya fault (Figure 8b). On the distribution map at a depth of 6 km, the velocity structure in the Minshan area to the north of Xueshan fault is characterized by trap-like distribution, whereas the division line between the high- and low-velocity anomaliesis shifted to the buried structure north of Huya fault. The low-velocity anomaly in the western part of BKB gradually enlarged, and alternating high- and low-velocity structures are observed in the northeastern part of SGB and Nanping Nappe tectonics at the southern tip of WQLOZ (Figure 8c). On the 9 km and 12 km depth distribution maps, the velocity anomaly in and around the Jiuzhaigou earthquake region shows zonation. The epicenter of the mainshock of the earthquake is located near the boundary between the high- and low-velocity anomalies and slightly tend toward the side of the high-velocity body (Figure 8 (d–e)). Such boundaries where medium properties undergo changes controlled by local structures may be favorable locations for the genesis and occurrence of strong earthquakes. The magnetotelluric inversion results obtained from field investigation teams from 188 dense arrays during their post-earthquake resurvey of the Jiuzhaigou area also show that the $M7.0$ Jiuzhaigou earthquake occurred at the boundary of the high and low resistivity and tend toward the side of the high-resistivity body (Sun XY et al., 2020). The latter results validate the reliability of our inversion results of the P-wave velocity structure.

As the inversion depth increases, patterns are observed in the distribution of crustal velocity structures in and around the Jiuzhaigou earthquake region. At a depth of 15 km, the low-velocity anomaly at northeastern SGB is more prominent, and the high-velocity anomaly in Nanping Nappe at the southern end of WQLOZ is expanding. A high-velocity anomaly appears in the region west of BKB (Figure 8f). At a depth of 18 km, the high-velocity anomaly to the west of BKB becomes more prominent. At MSM in the north of Xueshan fault, high- and low-velocity anomalies show strip-or belt-like distribution (Figure 8g), the high-velocity anomaly persists in Nanping Nappe (northeast of Jiuzhaigou earthquake region) and the region west of BKB. The low-velocity anomaly at northeastern SGB and MSM is expanding. Previous inversion results of the deep electrical structure also indicate the presence of high-resistivity strata, with resistivity ranging from hundreds to thousands of ohm·meters in the upper crust at a depth of approximately 20 km at the northeastern SGB. Going downward from there until deep in the Earth is the low-resistivity strata of middle and lower crust, with resistivity of several ohm·meters (Zhao GZ et al., 2012; Zhan Y et al., 2013). The Nan-
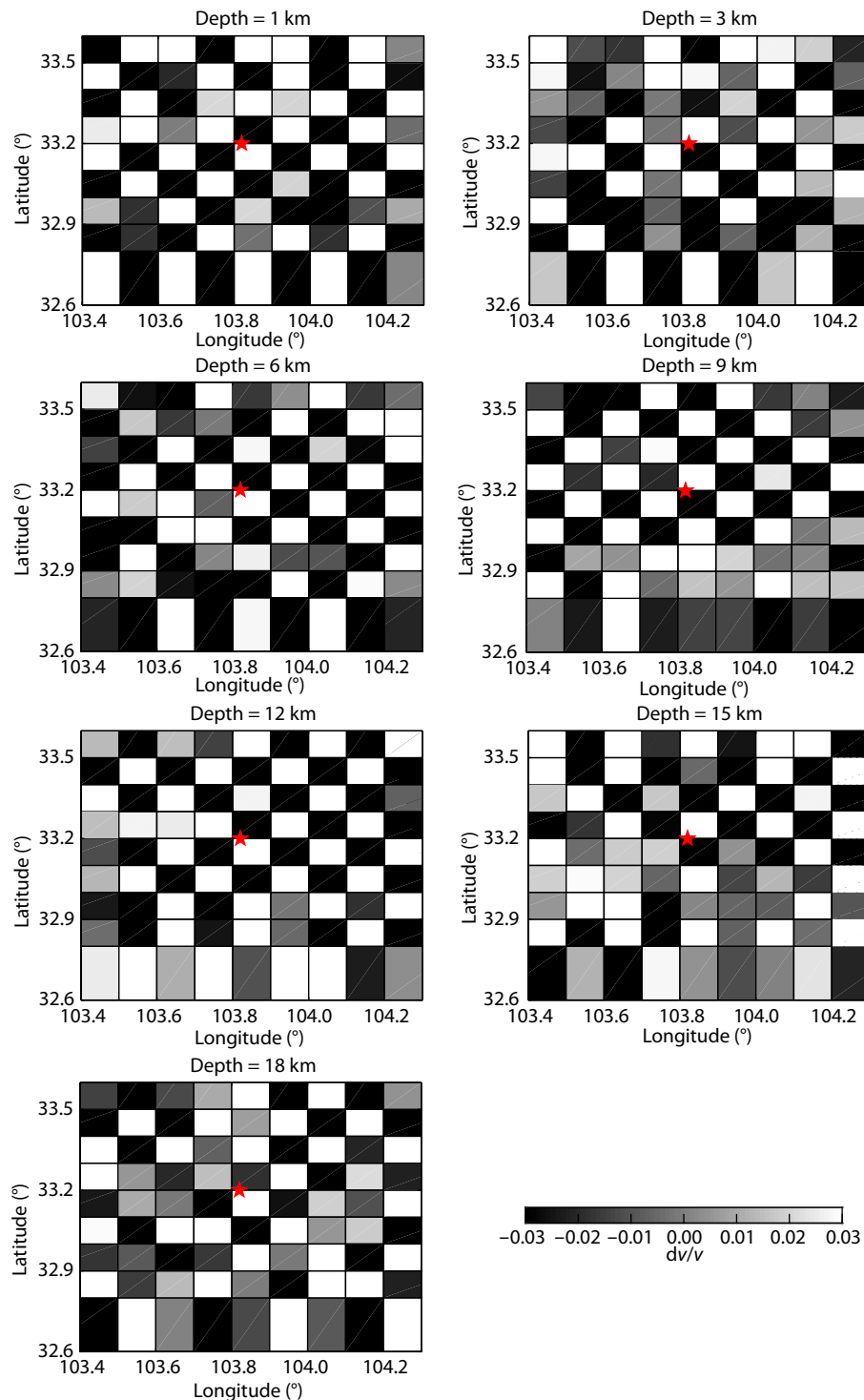
Figure 7. The results of the checkerboard resolution test at different depths. The layer depth is shown at the top of each figure. The red star shows the Jiuzhaigou mainshock.

ping Nappe tectonic belt in the southern margin of the WQLOZ shows high velocity characteristics, which is thought to hinder the northeastward migration of the crustal low-velocity of the northeastern SGB as extend into the MSM.

In addition to the lateral velocity structure plots, the SW-NE and NW-SE profiles across the *M*7.0 Jiuzhaigou earthquake region are presented here (Figure 9). On the SW–NE profile, obvious inhomo-

geneity is observed in the velocity structure of the MSM where the *M*7.0 Jiuzhaigou earthquake region is located. Prominent crustal low-velocity anomaly is found in the northeastern SGB to the west of MSM. No significant crustal low-velocity anomaly is observed at Nanping Nappe on the southern rim of the West Qinling Block (Figure 9a). The mainshock of the *M*7.0 Jiuzhaigou earthquake took place at the intersection of high- and low-velocity zones and in the brittle upper crust with low-velocity crustal zones as the un-
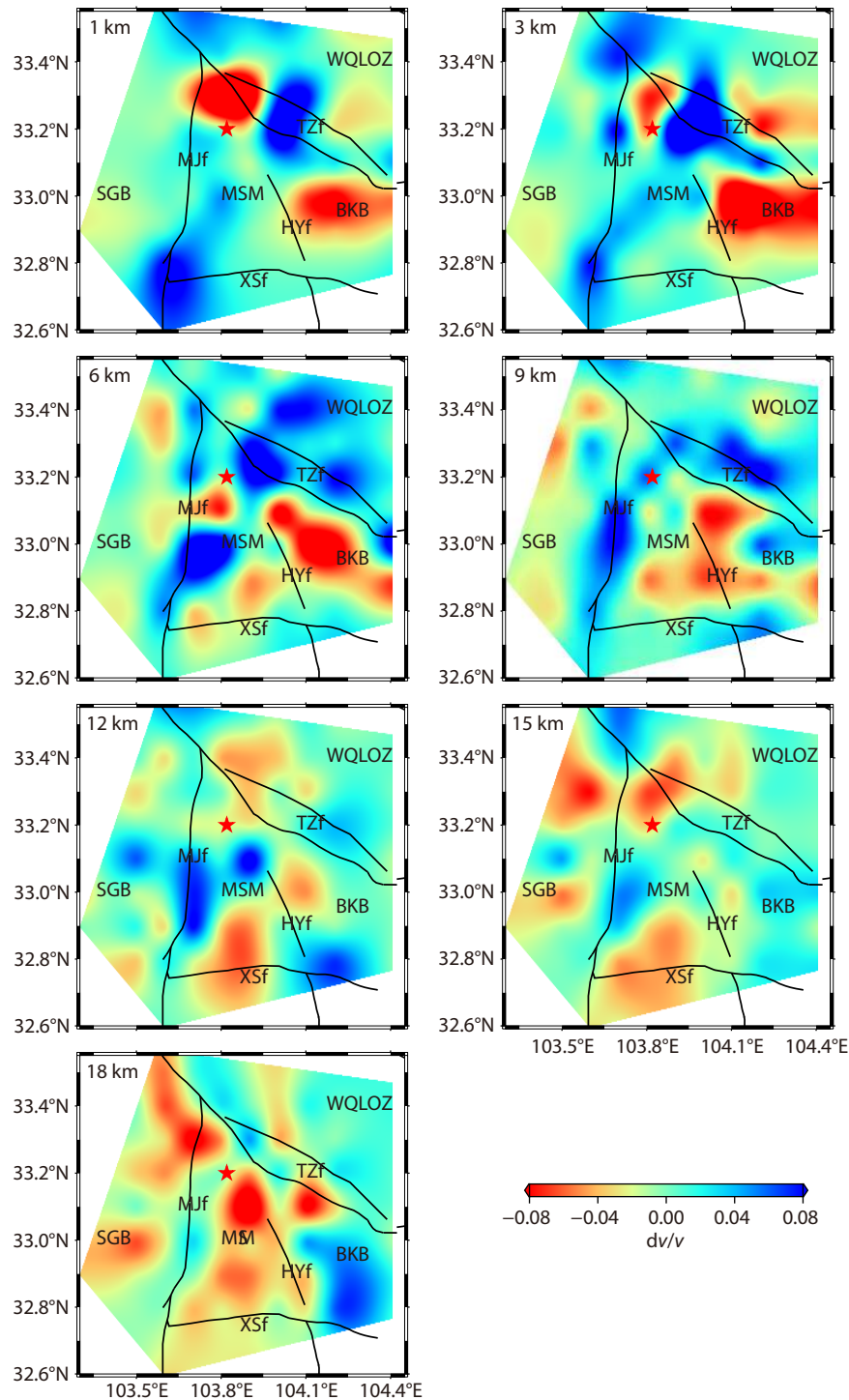
Figure 8. The horizontal slices of the tomography results. The layer depth is shown at the top left corner of each map figure. Red and blue colors denote low and high velocities, respectively. The faults represented by black curves and main block are the same as those in Figure 1; the red star shows the Jiuzhaigou mainshock.

derlying strata. In the NW-SE profile, the low-velocity zones of the northeastern SGB extend into MSM and move eastward (Figure 9b). They are blocked by the high velocity Nanping Nappe and BKB. As the entire Tibetan Plateau escapes eastward, the Minshan Block is compressed and uplifted, invoking left-lateral movement at the east side of Minshan relative to West Qiling Block and the BKB. Therefore, earthquakes happening on the east boundary of the Minshan Block are mainly strike-slip earthquakes.

4. Discussion

4.1 Characteristics of Velocity Structure and Distribution of Earthquake Sequence

There was no surface rupture caused by coseismic activity in the areas affected by the M7.0 Jiuzhaigou earthquake (Yi GX et al., 2017). Thus, the distribution pattern of the seismic sequence in
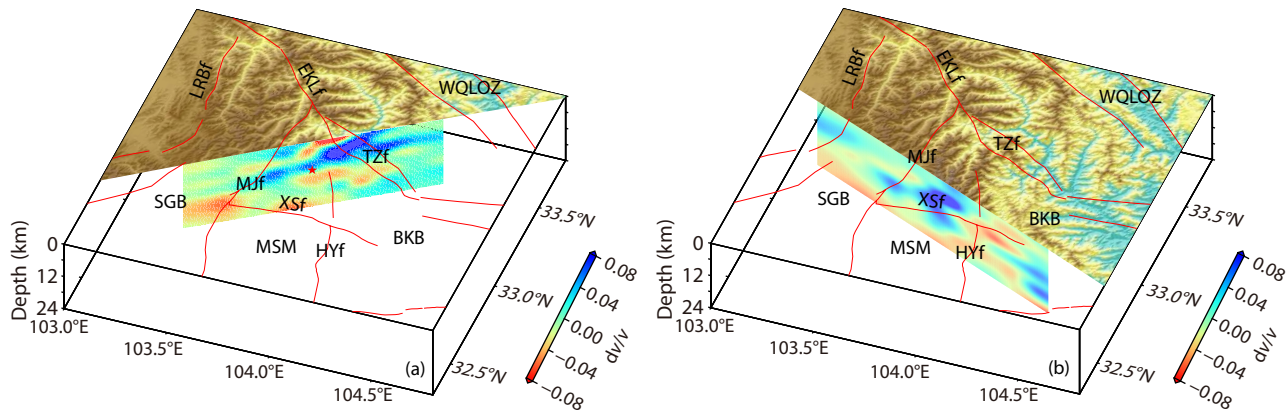
Li DH et al.: Upper crustal velocity of the M7.0 Jiuzhaigou earthquake region

Figure 9. The vertical sections of the tomography along two different directions. The velocity perturbation scale is shown on the right. Red and blue colors denote low- and high-velocity perturbations (in %), respectively.

the earthquake region and its relation to the structure of the deep medium and tectonic background is not yet clear. To understand further the relationship between the velocity structure of the *M*7.0 Jiuzhaigou earthquake region and the seismic sequence distribution, the seismic sequence distribution of the Jiuzhaigou Earthquake is plotted after relocation (Figure 10). The relocated aftershocks are distributed in the NW-SE direction in the area bounded by the Minjiang and Tazang faults. The long axis of the aftershock zone is about 40 km in length. The mainshock is located at the center of the aftershock zone, flanked by an aftershock belt about 20 km long on either side. Earthquake events are concentrated at the southern part of the aftershock belts and are more dispersed in the northern part. The AA′ profile for the focal depth along the NW-SE long axis shows the dominant distribution of focal depth at 5–20 km for the aftershock sequence. Obvious differences are also observed in the depth distribution between the northern and southern sections of the sequence: seismic events happen at a shallower depth in the northern section and are mainly concentrated at depths of 5–10 km; in the southern section, seismic events happen deeper, concentrated at depths of 10–20 km. For the depth profiles at different locations and perpendicular to the long axis, the BB′ and CC′ profile of the northern part of the aftershock zone shows a broad distribution of events, whereas the DD′ and EE′ profile of the southern part shows a narrower event distribution. Furthermore, the four lateral cross-sections all show nearly vertical seismogenic structures. The segmentation differences between the lateral cross-sections and vertical profiles may indicate a segmented seismogenic structure. The epicenters of the relocated aftershocks are distributed within a narrow zone along the NW-SE direction, between the nearly NS-trending Minjiang fault zone and the Tazang fault zone, The NW-SE-trending long axis of the aftershock zone is about 38 km; the *M*7.0 mainshock is located at the middle of the aftershock belt (Yi GX et al., 2017). The spatial distribution of the sequence is narrow and deep for the southern segment, but relatively wide and shallow for the northern segment (Long et al., 2019). Another important feature in the distribution of the earthquake sequence is its zonation, whose sequence distribution is another indication of the inhomogeneity in the crustal structure of the Jiuzhaigou earthquake region.

Based on the 3D P-wave velocity structure and aftershock se-

quence distribution, a close relationship is found between the spatial distribution of the *M*7.0 Jiuzhaigou earthquake sequence and the velocity structure in the earthquake region. For instance, In the 6 km depth velocity structure plot, there is a significant difference in the shallow velocity structure of the medium on the northeast and southwest sides of the Jiuzhaigou earthquake region; the earthquake sequence is distributed in the NW-SE direction along the division line between high-velocity and low-velocity anomalies and ends near the intersection of the Minjiang and Tazang faults (Figure 11a). This boundary zone of physical property change may be a location favorable for earthquake preparation and occurrence. At the 9 km depth, the epicenter of the Jiuzhaigou earthquake is still near the boundary between high- and low-velocity anomalies, tending slightly toward the side of the high-velocity body, although the distribution pattern of velocity anomalies has changed (Figure 11b). These unique velocity structure features were also reflected in previous studies of strong earthquake areas, such as those of the Lushan *M*7.0 earthquake, the Kangding *M*6.3 earthquake, and the Ludian *M*6.5 earthquake (Li DH et al., 2015a, b, 2019). Figure 11c shows that the southern segment of the *M*7.0 Jiuzhaigou earthquake sequence is located in the high-velocity anomaly area. This observation indicates that the high-speed area is prone to rupture, which is also the reason that the aftershock sequence in the southern part of the earthquake area is deeply distributed. The distribution characteristics of the aftershock sequence of the *M*6.0 Changning earthquake in 2019 also reinforce this point (Zuo KZ et al., 2020). Therefore, we can conclude that the spatial distribution of the Jiuzhaigou earthquake sequence is closely related to the velocity structure of the medium around the earthquake area. The inhomogeneous variation of the velocity structure of the Jiuzhaigou earthquake area and its surrounding medium is the deep structural factor controlling the spatial distribution of the mainshock and its sequence.

4.2 Deep Seismogenic Environment of Jiuzhaigou Earthquake Region

In the past 300 years, several earthquakes have occurred in the region around MSM, where the Jiuzhaigou earthquake region is situated. They have included the *M*7 Diexi earthquake in 1713, the *M*6½ Zhanglabei earthquake in 1748, the *M*6 Songpan earth-
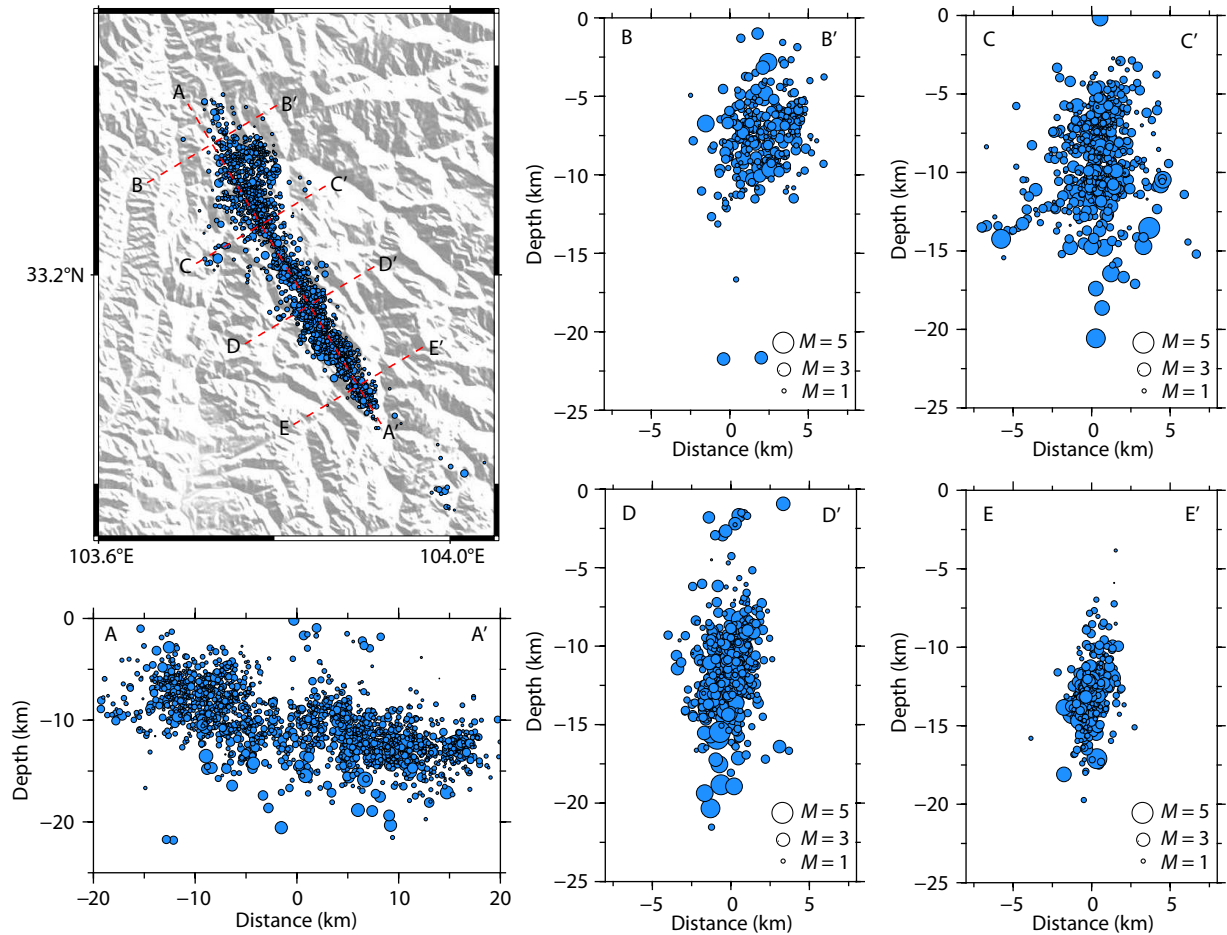
Figure 10. Distributions of epicenter after precise relocation and focal depth distributions of the B-B', C-C', D-D' and E-E' profiles.
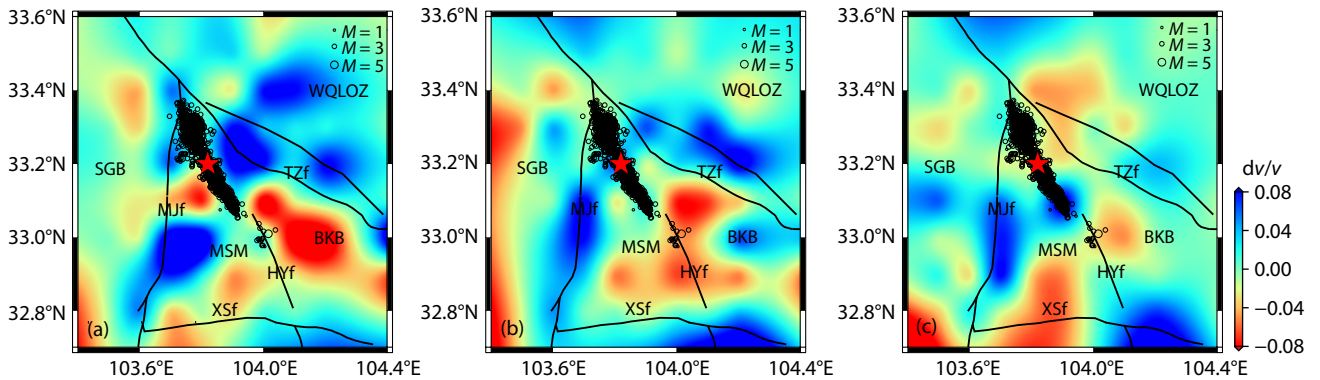

Figure 11. Velocity structure and distribution characteristics of aftershock sequence. Figures (a), (b), (c) denote 6, 9, and 12 km depths of horizontal slices of the tomography results, respectively.

quake in 1938, the M6¾ Zhangla earthquake in 1960, the M7½ Diexi earthquake in 1933 (as shown in Figure 1), and the M7.2, M6.7, and M7.2 Songpan–Pingwu earthquakes (Wen XZ, 2018). Important results have been achieved in recent years in geological and geophysical exploration in the region, such as the multi-scale inversion of the Bouguer gravity anomaly data, which revealed the existence of a significant low-value anomaly within the crust of MSM (Bi BT et al., 2016). Magnetotelluric soundings have indicated the presence of high-conductivity layer at depths of 10–

20 km at various places along the Minjiang and Longmenshan faults (Zhao GZ et al., 2012; Zhan Y et al., 2013). Geological and geophysical studies have shown that the east boundary of the crustal low-velocity anomaly (in the vicinity of the Minjiang fault) overlaps places where the mountain steepness and uplift rate change rapidly (Kirby et al., 2003). By analyzing InSAR and seismic waveform data, Sun JB et al. (2018) discovered the rupture of several major faults as a result of the Jiuzhaigou earthquake. However, the deep seismogenic environment and deep morpho-

Li DH et al.: Upper crustal velocity of the M7.0 Jiuzhaigou earthquake region

logy of the block-fault systems around the Jiuzhaigou earthquake region are yet to be clarified. Liu Z et al. (2017), in their profile study with short-period dense arrays, have suggested that the Tazang segment of the East Kunlun fault zone traverses the crust and leads to the formation of Moho discontinuity, whereas the deep seismic reflection profiling by Wang CS et al. (2011) and Gao R et al. (2014) along the Tangke–Hezuo profile of the contact zone between SGB and WQLOZ revealed that the East Kunlun fault zone does not cut through the Moho discontinuity; instead, it ends at the lateral delaminated layer at a depth of 35 km in the lower crust of the SGB, despite the dislocation and overlap observed in the Moho discontinuity of this region below the East Kunlun fault zone. Seismic imaging revealed a distinct low-velocity layer in the middle crust west of the Minjiang fault, whereas the middle and lower crust to east of the Minjiang fault shows relatively normal velocity (Shen WS et al., 2016). However, after the *M*7.0 Jiuzhaigou earthquake, inversion results of magnetotelluric soundings of the entire earthquake area suggest that the low-resistivity layer in the crust has extended to the east of the Minjiang fault (Sun XY et al., 2019, 2020). The conflicting reports described above illustrate the need for further study of the crustal velocity structure of the *M*7.0 Jiuzhaigou earthquake region, which would help to uncover the deep seismogenic environment and structure of the region.

The crustal soft media of the SGB on the eastern rim of the Tibetan Plateau extrudes eastward under the continuous northward push of the Indian Plate (Tapponnier et al., 1982). This material extrusion is blocked on the northeast and southeast by the rigid Ordos Block and the Sichuan Basin. The material migration changes direction and is rotated, and strain energy accumulates in the rotation zone. Fracture and strong earthquakes occur when the strength limit of the media is reached. The area affected by the *M*7.0 Jiuzhaigou earthquake is located in the south of the Tazang fault, which is in the transition zone from strike-slip to thrust. The seismogenic environment of the earthquake is affected by the material flow in the crust of the region (Xu XW et al., 2017b). The 3D P-wave velocity structure obtained in this study suggests that the low-velocity crustal layer of the northeastern SGB stretches into MSM, and they migrate to the northeast; but their tendency to emerge as a shallow layer is impeded by the high-velocity zone of Nanping Nappe and the BKB. Coincidentally, the inversion results of the 3D deep electrical structure also reveal the existence of low-resistivity layer in the crust of Minshan uplift, the buried depth of low resistivity layer gradually becomes shallow from Songpan Garze block to Minshan uplift. It indicates the trend of shallow surge along the northeast direction.

In conclusion, the deep velocity structure of the MSM, which is the location of the *M*7.0 Jiuzhaigou earthquake region, is characterized by mixed high-velocity and low-velocity anomalies. A significant crustal low-velocity anomaly is observed at the northeastern SGB, to the south of MSM, whereas there is no such crustal anomaly in Nanping Nappe at the southern rim of the West Qinling Block, to the north of MSM. The mainshock of the *M*7.0 Jiuzhaigou earthquake occurred at the boundary between the high- and low-velocity zones tending slightly toward the side of the high-velocity body, which is part of the brittle upper crust. Underneath it is a prominent crustal low-velocity zone. The crustal low-velocity layer of the earthquake region might be partially molten or in a state such that creep could happen readily. Strain energy can easily accumulate in the brittle upper crust; when the medium has reached its strength limit, it ruptures, leading to strong earthquakes.

4.3 Seismic Hazard Risk Evaluation in the Vicinity of the Earthquake Region

The P-wave velocity structure retrieved in this study reveals considerable lateral heterogeneity in the medium distribution of the crust in and around the *M*7.0 Jiuzhaigou earthquake region. Uneven distribution of high- and low-velocity structures was observed in the Tazang segment of the East Kunlun fault zone and the northern segment of Huya fault. This pattern can be expected to result in different magnitudes of stress accumulation in different segments of the fault. The epicenter of the mainshock of the *M*7.0 Jiuzhaigou earthquake is located near the boundary between distinct velocity anomalies, tending slightly toward the side of the high-velocity body. Such boundaries where the physical properties of media undergo local structure-controlled changes are generally thought to be favorable to the initiation and occurrence of medium and strong earthquakes. The *M*7.0 Jiuzhaigou earthquake happened in an area of enhanced stress left behind by the 2008 *M*8.0 Wenchuan earthquake (Toda et al., 2008). Based on changes in the Coulomb stress field, Xie ZJ et al. (2018) showed that the rupture caused by the Jiuzhaigou earthquake similarly enhances the stress fields at both ends of the seismogenic fault. Thus, it is important to stay vigilant to possible seismic hazards in the large seismic gap at the Maqu–Maqên segment of the East Kunlun fault zone (Wen XZ et al., 2007). There is a need for in-depth studies of the deep morphology of the Jiuzhaigou earthquake region and its surrounding fault zones, and the coupling between deep and shallow structures. This would aid a deep understanding of the characteristics of seismogenic structures. Detailed knowledge of the deep seismogenic environment in the region could be achieved, which would promote a more accurate evaluation of the potential for future seismic activities and thus the risk of serious seismic hazards.

5. Conclusion

Based on observation data recorded by the regional digital seismic networks and large-scale, dense mobile seismic array (China Array) for the northern section of the North–South Seismic Belt around the Jiuzhaigou earthquake region, we used the double-difference tomography method to invert 3D P-wave velocity structures for the upper crust of the *M*7.0 Jiuzhaigou earthquake region and its adjacent area, and have discussed the relationship between velocity structure and seismicity, deep seismogenic environment, and seismic hazard risk. The results are as follows:

(1) The P-wave velocity structure of the upper crust around the Jiuzhaigoug earthquake zone shows obvious lateral inhomogeneity; the distribution characteristics of the shallow P-wave velocity structure are closely related to surface geological structure and formation lithology. Trap-like low-velocity anomalies are observed at the intersection of the Minjiang and Tazang faults; in the

western part of the BKB, the east and west sides of the northern section of the Huya fault show low- and high-velocity structures, respectively.

(2) The distribution of the relocated Jiuzhaigou M7.0 earthquake sequence are closely related to the velocity structure of the upper crust. The earthquake sequence is distributed along the NW-SE direction and ends near the intersection of the Minjiang and Tazang faults, and the spatial distribution of sequence shows zonal characteristics. The inhomogeneous variation of the velocity structure of the Jiuzhaigou earthquake area and its surrounding medium is the deep structural factor controlling the spatial distribution of the mainshock and its sequence.

(3) The 3D P-wave velocity structure obtained in this study also suggests that the low-velocity crustal material of the northeastern SGB stretches into MSM, in the process of northeastward migration, on the one hand, it has the trend of surging to the shallow layer, on the other hand, it is impeded by the high-velocity zone of the Nanping Nappe and BKB. The mainshock of the M7.0 Jiuzhaigou earthquake occurred in the upper crust. Underneath it is a prominent crustal low-velocity layer. Strain energy can easily accumulate in the brittle upper crust; when the medium has reached its strength limit, it ruptures, leading to strong earthquakes.

(4) Our results reveal considerable lateral heterogeneity in the medium distribution of the upper crust in and around the M7.0 Jiuzhaigou earthquake region. Uneven distribution of high- and low-velocity structures were observed in the Tazang segment of the East Kunlun fault zone. The Jiuzhaigou earthquake enhances the stress fields at both ends of the seismogenic fault. Thus, it is important to stay vigilant to possible seismic hazards in the large seismic gap at the Maqu–Maqên segment of the East Kunlun fault zone.

References

Allam, A. A., Ben-Zion, Y., Kurzon, I., and Vernon, F. (2014). Seismic velocity structure in the hot springs and trifurcation areas of the San Jacinto fault zone, California, from double-difference tomography. *Geophys. J. Int.*, 198(2), 978–999. https://doi.org/10.1093/gji/ggu176

Bi, B. T., Hu, X. Y., Li, L. Q., Zhang, H. L., Liu, S., and Cai, J. C. (2016). Multi-scale analysis to the gravity field of the northeastern Tibetan plateau and its geodynamic implications. *Chin. J. Geophys.*, 59(2), 543–555. https://doi.org/10.6038/cjg20160213

Cunningham, W. D., and Mann, P. (2007). Tectonics of strike-slip restraining and releasing bends. *Geol. Soc. London Spec. Publ.*, 290(1), 1–12. https://doi.org/10.1144/SP290.1

Ding, Z. F. (2011). China seismic science array exploration-South section of the North South seismic belt. *Seismic Sci. Technol. Int. Exchange*, 2, 36–39.

Eberhart-Phillips, D. (1986). Three-dimensional velocity structure in northern California Coast Ranges from inversion of local earthquake arrival times. *Bull. Seismol. Soc. Am.*, 76(4), 1025–1052.

Eberhart-Phillips, D. (1993). Local Earthquake Tomography: Earthquake Source Regions. In H. M. Iyer, et al. (Eds.), *Seismic Tomography*: *Theory and Practice* (pp. 613-643). London: Chapman and Hall.

Fang, L. H., Wu, J. P., Su, J. R., Wang, M. M., Jiang, C., Fan, L. P., Wang, W. L., Wang, C. Z., and Tan, X. L. (2018). Relocation of mainshock and aftershock sequence of the M_S7.0 Sichuan Jiuzhaigou earthquake. *Chin. Sci. Bull.*, 63(7), 649–662. https://doi.org/10.1360/N972017-01184

Gao, R., Wang, H. Y., Zeng, L. S., Zhang, J. S., Guo, T. L., Li, Q. S., Li, W. H., Li, P. W., and Guan, Y. (2014). The crust structures and the connection of the Songpan block and West Qinling orogen revealed by the Hezuo-Tangke deep seismic reflection profiling. *Tectonophysics*, 634, 227–236. https://doi.org/10.1016/j.tecto.2014.08.014

Hansen, P. C. (1992). Analysis of discrete ill-posed problems by means of the L-curve. *SIAM Rev.*, 34(4), 561–580. https://doi.org/10.1137/1034115

Hansen, P. C., and O'Leary, D. P. (1993). The use of the L-curve in the regularization of discrete ill-posed problems. *SIAM J. Sci. Comput.*, 14(6), 1487–1503. https://doi.org/10.1137/0914086

Hofstetter, R., Dorbath, C., and Calò, M. (2012). Crustal structure of the Dead Sea Basin from local earthquake tomography. *Geophys. J. Int.*, 189(1), 554–568. https://doi.org/10.1111/j.1365-246X.2012.05369.x

Ji, L. Y., Liu, C. J., Xu, J., Liu, L., Long, F., and Zhang, Z. W. (2017). InSAR observation and inversion of the seismogenic fault for the 2017 Jiuzhaigou M_S7.0 earthquake in China. *Chin. J. Geophys.*, 60(10), 4069–4082. https://doi.org/10.6038/cjg20171032

Kirby, E., Whipple, K. X., Tang, W. Q., and Chen, Z. L. (2003). Distribution of active rock uplift along the eastern margin of the Tibetan Plateau: Inferences from bedrock channel longitudinal profiles. *J. Geophys. Res.*, 108(B4), 2217. https://doi.org/10.1029/2001JB000861

Li, C. X., Xu, X. W., Wen, X. Z., Zheng, R. Z., Chen, G. H., Yang, H., An, Y. F., and Gao, X. (2011). Rupture segmentation and slip partitioning of the mid-eastern part of the Kunlun Fault, north Tibetan Plateau. *Sci. China Earth Sci.*, 54(11), 1730–1745. https://doi.org/10.1007/s11430-011-4239-5

Li, D. H., Ding, Z. F., Wu, P. P., Zheng, C., Ye, Q. D., and Liang, M. J. (2015a). The deep seismogenic environment of the southeastern section of the Xianshuihe fault zone and the 2014 Kangding M_S6.3 earthquake. *Chin. J. Geophys.*, 58(6), 1941–1953. https://doi.org/10.6038/cjg20150610

Li, D. H., Wu, P. P., and Ding, Z. F. (2015b). Tomography of the three dimensional P-wave velocity structure in the source region of the M_S7.0 Lushan, Sichuan, earthquake and its surrounding areas. *Acta Seismol. Sin.*, 37(3), 371–385. https://doi.org/10.11939/jass.2015.03.001

Li, D. H., Ding, Z. F., Wu, P. P., Liang, M. J., Wu, P., Gu, Q. P., and Kang, Q. Q. (2019). Deep structure of the Zhaotong and Lianfeng fault zones in the eastern segment of the Sichuan-Yunnan border and the 2014 Ludian M_S6.5 earthquake. *Chin. J. Geophys.*, 62(12), 4571–4587. https://doi.org/10.6038/cjg2019M0450

Li, D. H., Zhan, Y., Ding, Z. F., Gao, J. Y., Wu, P. P., Meng, L. Y., Sun, X. Y., and Zhang, X. (2021). Upper crustal velocity and seismogenic environment of the Changning M_S6.0 earthquake region in Sichuan, China. *Chin. J. Geophys.*, 64(1), 18–35. https://doi.org/10.6038/cjg2021O0241

Liang, J. H., Sun, L., and Liu, J. (2018). A high precision relocation study of the M_S7.0 Jiuzhaigou earthquake and the aftershocks occurred in 2017. *Chin. J. Geophys.*, 61(5), 2152–2162. https://doi.org/10.6038/cjg2018L0604

Liang, S. S., Lei, J. S., Xu, Z. G., Xu, X. W., Zou, L. Y., Liu, J. G., and Chen, H. F. (2018). Relocation of aftershocks of the 2017 Jiuzhaigou, Sichuan, M_S7.0 earthquake and inversion for focal mechanism of the mainshock. *Chin. J. Geophys.*, 61(5), 2163–2175. https://doi.org/10.6038/cjg2018L0508

Liu, Z., Tian, X. B., Gao, R., Wang, G. C., Wu, Z. B., Zhou, B. B., Tan, P., Nie, S. T., Yu, G. P., … Xu, X. (2017). New images of the crustal structure beneath eastern Tibet from a high-density seismic array. *Earth Planet. Sci. Lett.*, *480*, 33–41. https://doi.org/10.1016/j.epsl.2017.09.048

Long, F., Yi, G. X., Wang, S. W., Qi, Y. P., and Zhao, M. (2019). Geometry and tectonic deformation of the seismogenic structure for the 8 August 2017 M_S 7.0 Jiuzhaigou earthquake sequence, northern Sichuan, China. *Earth Planet. Phys.*, *3*(3), 253–267. https://doi.org/10.26464/epp2019027

Ma, X., Westman, E. C., Fahrman, B. P., and Thibodeau, D. (2016). Imaging of temporal stress redistribution due to triggered seismicity at a deep nickel mine. *Geomechan. Energy Environ.*, *5*, 55–64. https://doi.org/10.1016/j.gete.2016.01.001

Min, G., Wang, X. B., Xia, S. B., Zhou, J., Zhang, B., Cai, X. L., and Liang, S. Q. (2017). Electrical structure of middle and upper crust beneath the Minshan uplift zone and central section of the West Qinling orogenic zone. *Chin. J. Geophys.*, *60*(6), 2397–2413. https://doi.org/10.6038/cjg20170629

Okada, T., Yaginuma, T., Umino, N., Matsuzawa, T., Hasegawa, A., Zhang, H. J., and Thurber, C. H. (2006). Detailed imaging of the fault planes of the 2004 Niigata-Chuetsu, central Japan, earthquake sequence by double-difference tomography. *Earth Planet. Sci. Lett.*, *244*(1–2), 32–43. https://doi.org/10.1016/j.epsl.2006.02.010

Okada, T., Hasegawa, A., Suganomata, J., Umino, N., Zhang, H. J., and Thurber, C. H. (2007). Imaging the heterogeneous source area of the 2003 M6.4 northern Miyagi earthquake, NE Japan, by double-difference tomography. *Tectonophysics*, *430*(1-4), 67–81. https://doi.org/10.1016/j.tecto.2006.11.001

Qin, J. F., Lai, S. C., Zhang, G. W., Diwu, C. R., and Li, Y. F. (2008). Zircon LA-ICP-MS U-Pb dating of the Longkang ignimbrite in the Jiuzhaigou area, Sichuan, China: Evidence of the westward Extension of the Mianlüe suture. *Geol. Bull. China*, *27*(3), 345–350. https://doi.org/10.3969/j.issn.1671-2552.2008.03.005

Shen, W. S., Ritzwoller, M. H., Kang, D., Kim, Y. H., Lin, F. C., Ning, J. Y., Wang, W. T., Zheng, Y., and Zhou, L. Q. (2016). A seismic reference model for the crust and uppermost mantle beneath China from surface wave dispersion. *Geophys. J. Int.*, *206*(2), 954–979. https://doi.org/10.1093/gji/ggw175

Spakman W, Van Der Lee S, Van Der Hilst R. (1993). Travel-time tomography of the European-Mediterranean mantle down to 1400 km. *Physics of the Earth and Planetary Interiors*, *79*(1–2), 3–74. https://doi.org/10.1016/0031-9201(93)90142-V

Sun, J. B., Yue, H., Shen, Z. K., Fang, L. H., Zhan, Y., and Sun, X. Y. (2018). The 2017 Jiuzhaigou earthquake: a complicated event occurred in a young fault system. *Geophys. Res. Lett.*, *45*(5), 2230–2240. https://doi.org/10.1002/2017GL076421

Sun, X. Y., Zhan, Y., Zhao, L. Q., Chen, X. B., Sun, J. B., Li, C. X., Cui, T. F., and Han, J. (2019). Electrical structure of the Kunlun-Qinling fault system, northeastern Tibetan Plateau, inferred from 3–D inversion of magnetotelluric data. *J. Asian Earth Sci.*, *181*, 103910. https://doi.org/10.1016/j.jseaes.2019.103910

Sun, X. Y., Zhan, Y., Unsworth, M., Egbert, G., Zhang, H. P., Chen, X. B., Zhao, G. Z., Sun, J. B., Zhao, L. Q., … Han, J. (2020). 3-D Magnetotelluric imaging of the easternmost Kunlun fault: Insights into strain partitioning and the seismotectonics of the Jiuzhaigou M_S7.0 earthquake. *J. Geophys. Res. Solid Earth*, *125*(5), e2020JB019731. https://doi.org/10.1029/2020JB019731

Tapponnier, P., Peltzer, G., Le Dain, A. Y., Armijo, R., and Cobbold, P. (1982). Propagating extrusion tectonics in Asia: new insights from simple experiments with plasticine. *Geology*, *10*(12), 611–616. https://doi.org/10.1130/0091-7613(1982)10<611:PETIAN>2.0.CO;2

Thurber, C., Roecker, S., Zhang, H. J., Baher, S., and Ellsworth, W. (2004). Fine-scale structure of the San Andreas fault zone and location of the SAFOD target earthquakes. *Geophys. Res. Lett.*, *31*(12), L12S02. https://doi.org/10.1029/2003GL019398

Thurber, C. H., Brocher, T. M., Zhang, H. J., and Langenheim, V. E. (2007). Three-dimensional P wave velocity model for the San Francisco Bay region, California. *J. Geophys, Res.*, *112*(B7), B07313. https://doi.org/10.1029/2006JB004682

Toda, S., Lin, J., Meghraoui, M., and Stein, R. S. (2008). 12 May 2008 M=7.9 Wenchuan, China, earthquake calculated to increase failure stress and seismicity rate on three major fault systems. *Geophys. Res. Lett.*, *35*(17),

L17305. https://doi.org/10.1029/2008GL034903

Waldhauser, F., and Ellsworth, W. L. (2000). A double-difference earthquake location algorithm: method and application to the northern Hayward fault, California. *Bull. Seismol. Soc. Am.*, *90*(6), 1353–1368. https://doi.org/10.1785/0120000006

Wang, C. S., Gao, R., Yin, A., Wang, H. Y., Zhang, Y. X., Guo, T. L., Li, Q. S., and Li, Y. L. (2011). A mid-crustal strain-transfer model for continental deformation: a new perspective from high-resolution deep seismic-reflection profiling across NE Tibet. *Earth Planet. Sci. Lett.*, *306*(3–4), 279–288. https://doi.org/10.1016/j.epsl.2011.04.010

Watkins, W. D., Thurber, C. H., Abbott, E. R., and Brudzinski, M. R. (2018). Local earthquake tomography of the Jalisco, Mexico region. *Tectonophysics*, *724-725*, 51–64. https://doi.org/10.1016/j.tecto.2018.01.002

Wen, X. Z., Yi, G. X., and Xu, X. W. (2007). Background and precursory seismicities along and surrounding the Kunlun fault before the M_S8.1, 2001, Kokoxili earthquake, China. *J. Asian Earth Sci.*, *30*, 63–72. https://doi.org/10.1016/j.jseaes.2006.07.008

Wen, X. Z. (2018). The 2008 Wenchuan, 2013 Lushan and 2017 Jiuzhaigou earthquakes, Sichuan, in the last more than one thousand years of rupture history of the eastern margin of the Bayan Har block. *Acta Seismol. Sin.*, *40*(3), 255–267. https://doi.org/10.11939/jass.20170211

Wu, H. B., Shen, X. L., Wang, J., Zhao, L. Y., and Chen, J. H. (2018). Three-dimensional velocity structure of upper crust in the Three Gorges Reservoir area derived from double-difference tomography. *Chin. J. Geophys.*, *61*(7), 2802–2814. https://doi.org/10.6038/cjg2018L0345

Xie, Z. J., Zheng, Y., Yao, H. J., Fang, L. H., Zhang, Y., Liu, C. L., Wang, M. M., Shan, B., Zhang, H. P., … Song, M. Q. (2018). Preliminary analysis on the source properties and seismogenic structure of the 2017 M_S7.0 Jiuzhaigou earthquake. *Sci. China Earth Sci.*, *61*(3), 339–352. https://doi.org/10.1007/s11430-017-9161-y

Xu, L. S., Zhang, X., and Li, C. L. (2018). Which velocity model is more suitable for the 2017 M_S7.0 Jiuzhaigou earthquake?. *Earth Planet. Phys.*, *2*(2), 163–169. https://doi.org/10.26464/epp2018016

Xu, T., Zhang, M. H., Tian, X. B., Zheng, Y., Bai, Z. M., Wu, C. L., Zhang, Z. J., and Teng, J. W. (2014). Upper crustal velocity of Lijiang-Qingzhen profile and its relationship with the seismogenic environment of the M_S6.5 Ludian earthquake. *Chin. J. Geophys.*, *57*(9), 3069–3079. https://doi.org/10.6038/cjg20140932

Xu, X. W., Chen, G. H., Wang, Q. X., Chen, L. C., Ren, Z. K., Xu, C., Wei, Z. Y., Lu, R. Q., Tan, X. B., … Shi, F. (2017a). Discussion on seismogenic structure of Jiuzhaigou earthquake and its implication for current strain state in the southeastern Qinghai-Tibet Plateau. *Chin. J. Geophys.*, *60*(10), 4018–4026. https://doi.org/10.6038/cjg20171028

Xu, X. W., Wu, X. Y., Yu, G. H., Tan, X. B., and Li, K. (2017b). Seismo-Geological signatures for identifying $M \geq 7.0$ earthquake risk areas and their premilimary application in Mainland China. *Seismol. Geol.*, *39*(2), 219–275.

Yang, Y., and Chang, L. J. (2018). Variations of shear wave splitting in the source region of the 2017 Jiuzhaigou M_S7.0 earthquake. *Chin. J. Geophys.*, *61*(5), 2088–2098. https://doi.org/10.6038/cjg2018M0174

Yi, G. X., Long, F., Liang, M. J., Zhang, H. P., Zhao, M., Ye, Y. Q., Zhang, Z. W., Qi, Y. P., Wang, S. W., … Su, J. R. (2017). Focal mechanism solutions and seismogenic structure of the 8 August 2017 M7.0 Jiuzhaigou earthquake and its aftershocks, northern Sichuan. *Chin. J. Geophys.*, *60*(10), 4083–4097. https://doi.org/10.6038/cjg20171033

Zhan, Y., Zhao, G. Z., Unsworth, M., Wang, L. F., Chen, X. B., Li, T., Xiao, Q. B., Wang, J. J., Tang, J., … Wang, Y. Z. (2013). Deep structure beneath the southwestern section of the Longmenshan fault zone and seimogenetic context of the 4.20 Lushan M_S7.0 earthquake. *Chin. Sci. Bull.*, *58*(28-29), 3467–3474. https://doi.org/10.1007/s11434-013-6013-x

Zhang, H. J., and Thurber, C. H. (2003). Double-difference tomography: the method and its application to the Hayward fault, California. *Bull. Seismol. Soc. Am.*, *93*(5), 1875–1889. https://doi.org/10.1785/0120020190

Zhang, H. J., and Thurber, C. (2006). Development and applications of double-difference seismic tomography. *Pure. Appl. Geophys.*, *163*(2-3), 373–403. https://doi.org/10.1007/s00024-005-0021-y

Zhang, H. P., Liu, S. F., Yang, N., Zhang, Y. Q., and Zhang, G. W. (2006). Geomorphic characteristics of the Minjiang drainage basin (eastern Tibetan Plateau) and its tectonic implications: New insights from a digital elevation model study. *Island Arc*, *15*(2), 239–250. https://doi.org/10.1111/j.1440-1738.2006.00524.x

Zhang, X., Feng, W. P., Xu, L. S., and Li, C. L. (2017). The source-process inversion and the intensity estimation of the 2017 M_s7.0 Jiuzhaigou earthquake. *Chin. J. Geophys.*, *60*(10), 4105–4116. https://doi.org/10.6038/cjg20171035

Zhao, C. P. (2006). *Study on Seismological Methods for the Characteristics of Jiashi Focal Area in Xinjiang from 1997 to 2003*. Institute of Geophysics, China Earthquake Administration.

Zhao, G. Z., Unsworth, M. J., Zhan, Y., Wang, L. F., Chen, X. B., Jones, A. G., Tang, J., Xiao, Q. B., Wang, J. J., … Zhang, J. H. (2012). Crustal structure and rheology of the Longmenshan and Wenchuan Mw 7.9 earthquake epicentral area from magnetotelluric data. *Geology*, *40*(12), 1139–1142. https://doi.org/10.1130/G33703.1

Zhao, X. L., Deng, Q. D., and Chen, S. F. (1994). Tectonic geomorphology of the Minshan uplift in western Sichuan, southwestern China. *Seismol. Geol.*, *16*(4), 429–439.

Zuo, K. Z., Zhao, C. P., and Zhang, H. (2020). 3D crustal structure and seismicity characteristics of Changning–Xingwen Area in the Southwestern Sichuan Basin, China. *Bull. Seismol. Soc. Am.*, *110*(5), 2154–2167. https://doi.org/10.1785/0120200085